https://doi.org/10.38124/ijisrt/25nov007

# Analytical and Numerical Modelling of Electron Transmission Probability Through Quantum Tunnelling Barriers in Nanoscale Diodes

## Pratham Dungrani<sup>1</sup>

<sup>1</sup>Delhi Private School, Dubai

Publication Date: 2025/11/15

Abstract: Quantum tunnelling becomes critical in nanoelectronic devices as dimensions approach or fall below the electron mean free path, wherein the classical transport models are no longer sufficient to describe carrier behavior. Accordingly, transmission of electrons across barriers is analyzed in nanodiodes within this paper using three main approaches: the Schrödinger Equation Method, the Wentzel-Kramers-Brillouin (WKB) approximation, and the Transfer Matrix Method. These methods have been applied to various tunneling situations involving barriers of different height and width, as well as semiconductor material interfaces representative of state-of-the-art device architectures in capturing the wavelike nature of electron transport typical at nanometric scales.

A comparison is carried out in regard to the accuracy, efficiency of computation, and physical insights gained through each approach. Strengths and weaknesses of the above-mentioned techniques will be considered in view a variety of barrier profiles and device structures. Calculations based on self-consistent potentials in Si and GaAs hetero-structures exhibit strong exponential behavior of the tunneling current and barrier parameters. Consistency between methods appears only under the following special conditions of barrier variation.

These results are discussed in relation to the emerging importance of a new class of tunneling-based devices: MIMs, RTDs, and TFETs, all promising for next-generation electronic and optoelectronic systems. These findings provide a conceptual and practical basis for the understanding and designing of nanoscale devices where tunneling is a dominant transport mechanism, adding an important comprehensive perspective to quantum transport modeling in nanoelectronics.

**Keywords:** Quantum Tunneling, Nanoelectronics, Schrödinger Equation, WKB Approximation, Transfer Matrix Method, Tunneling Probabilities, Metal—Insulator—Metal Diodes, Resonant Tunneling Diodes, Tunneling Field-Effect Transistors, Electron Transmission, Potential Barriers, Nanoscale Devices, Computational Efficiency, Silicon, Gallium Arsenide, Self-Consistent Potential Profiles, Quantum Mechanics in Nanoelectronics, Device Modeling, Barrier Height, Barrier Width, Material Interfaces, Numerical Simulations.

**How to Cite:** Pratham Dungrani (2025). Analytical and Numerical Modelling of Electron Transmission Probability Through Quantum Tunnelling Barriers in Nanoscale Diodes. *International Journal of Innovative Science and Research Technology*, 10(11), 440-454. https://doi.org/10.38124/ijisrt/25nov007

#### I. INTRODUCTION

The development of today's electronics has been led very strongly by the relentless scaling down of devices based on the expectations of Moore's Law. With the device transistor size scaling down to the nanometer scale, the physical basis of current transport has gradually moved away from classical drift diffusion to quantum-mechanical wave phenomena. Such effects as quantum tunneling, interference of the wave function, and quantum confinement were long deemed insignificant. Yet today they can profoundly influence the behavior and performance of devices at the nanoscale.

Among the new phenomena that emerged based on the quantum world, quantum tunneling has become one of the most remarkable and useful effects. In traditional electronics devices, quantum tunneling has been recognized as a problematic current flow across thin oxide barriers in MOSFETs, capacitors, and non-volatile memories. On the other hand, when specifically designed, quantum tunneling phenomena are the basis for the operation of many innovative devices like resonant tunneling diodes (RTDs), metal–insulator–metal (MIM) diodes, quantum cascade lasers, and tunneling field-effect transistors (TFETs). This specifically indicates the important role given to the suppression as well as the usage of quantum tunneling.

ISSN No: -2456-2165

https://doi.org/10.38124/ijisrt/25nov007

From a theoretical point of view, classical physics would predict the total reflection of the electron if the potential barrier exceeded the kinetic energy of the electron. On the contrary, the wave-particle duality formalism of quantum mechanics predicts the possibility of penetration across the barrier. This effect predicted by the time-independent Schrödinger equation. This positive probability of tunneling for energies below the barrier height serves as the basis for the definition of the tunneling effect. The exponentially decaying wave function in the barrier region determines the natural barrier-dependent sensitivity of the process of tunneling to the thickness and barrier geometry-dependent transport mechanism. As a consequence, even sub-angström-scale changes in barrier width can produce large discrepancies in the probability of electron transmission.

The early analytical basis for the theory of tunneling was developed by Fowler and Nordheim (1928), who considered the field emission across a triangular barrier under a strong electric field. This effort became the basis for the extensions made by Simmons (1963), tracing the theory of tunneling across thin insulating barriers between metal electrodes. This classical treatment became the basis for the theory of MIM tunneling. Later analyses involved barrier shapes that were square-like, trapezoidal, and multiple barrier-like structures, in which the semi-classical formulation of the Wentzel-Kramers-Brillouin (WKB) approximation became applicable due to slowly varying barrier shapes. However, the semi-classical formulation has some limitations when used for interfaces.multi-barrier systems, or hetero-structures in which the material parameters change discretely.

The development of nanofabrication techniques and atomic-scale heterostructure designs, the use of numerical methods has become indispensable for modeling the process of electron tunneling. The solution of the time-independent Schrödinger equation provides exact expressions for the transmission probabilities. This method has the advantage of producing exact results. Another method used to solve the aforementioned equations is the Transfer Matrix Method (TMM), multi-layered systems, and effective mass variation calculations with high numerical stability. These techniques allow accurate modeling of resonant tunneling phenomena involving Bias-dependent barrier lowering heterojunction transport: important phenomena in more advanced device structures.

Simultaneously, the area has also witnessed the emergence of atomic-scale modeling schemes like the non-equilibrium Green's function formalism (NEGF) and density functional theory (DFT). Although such schemes offer unprecedented levels of accuracy because of the inclusion of atomic potentials and many-body interactions, their computational requirements generally preclude their usability in device simulations. Consequently, the following imperative arises for the development of hybrid modeling tools that can combine the analytical advantages of semiclassical approaches with the numerically rigorous solutions obtained from matrices.

Current research underlines the importance of the predictive tunneling modeling approach not only as a tool for the optimization of devices but also for material studies and quantum capacitance design. As transport phenomena continue to demonstrate the dominance of quantum tunneling currents at the nano-scale cross-validate, and interpret results across different modeling paradigmas.

The present work addresses this need by presenting a comprehensive comparative framework for analyzing electron transmission through quantum tunneling barriers in nanoscale diodes. Specifically, it evaluates three foundational approaches—the Schrödinger Equation Method (SE), the WKB approximation, and the Transfer Matrix Method (TMM)—across multiple barrier profiles, material systems, and bias conditions. By systematically assessing the accuracy, computational efficiency, and physical interpretability of each method, this study establishes a quantitative benchmark for tunneling analysis in nanoscale and quantum electronic devices. Furthermore, the framework elucidates how parameters such as barrier height (V<sub>0</sub>), applied bias (Vb), effective mass, and barrier geometry collectively influence transmission probability, thereby providing deep insights into device-level tunneling control.

Ultimately, this investigation contributes to the growing field of quantum transport modeling, offering both theoretical clarity and practical guidance for researchers and engineers designing the next generation of quantum-enabled nanoelectronic systems.

## II. THEORETICAL FRAMEWORK

## > Quantum Mechanical Basis

An electron of energy E moving through a onedimensional potential V(x) obeys the time-independent Schrödinger equation:

$$\frac{d^2\Psi}{dx^2} + \frac{2m}{h^2} [E - v(x)] \psi(x) = 0$$

Where where  $\psi(x)$  is the wavefunction, m is the effective electron mass, and  $\hbar$  the reduced Planck's constant.

For regions of constant potential, the general solution is:

$$\psi(x) = Ae^{ikx} + Be^{-ikx},$$

where 
$$k = \frac{\sqrt{2m(E-V)}}{h^2}$$

Continuity of  $\psi(x)$  and  $d\psi/dx$  ensures conservation of probability current.

For an incident wave from the left, the transmission (T) and reflection (R) coefficients are obtained by boundary matching:

$$T = \frac{|F|^2}{|A|^2} \frac{k_3}{k_1}, R = \frac{|B|^2}{|A|^2}$$

ISSN No: -2456-2165

https://doi.org/10.38124/ijisrt/25nov007

Where k1 and k3 denote the wave numbers in the incident and transmitted regions respectively

#### ➤ WKB Approximation

The WKB (Wentzel-Kramers-Brillouin) approximation provides an analytical approach for smoothly varying potentials.

Assuming V(x) changes slowly relative to the de-Broglie wavelength, the solution is:

$$\Psi(x) \approx \frac{C}{\sqrt{k(x)}} e^{\pm i \int_{x_0}^x k(x') dx'}$$

For tunneling through a classically forbidden region (V(x)>E):

$$T_{WKB} \approx exp[-2\int_{x_1}^{x_2} \kappa(x) dx]$$

Where 
$$\kappa(x) = \frac{\sqrt{2m(V(x)-E)}}{h^2}$$

And  $x_1$ ,  $x_2$  are classical turning points.

WKB is computationally efficient and physically intuitive but loses accuracy near abrupt potential transitions and fails for multi-barrier or resonant structures.

## > Transfer Matrix Method (TMM)

The TMM is a numerically robust approach for arbitrary or multilayer potential profiles.

Each layer i with potential  $V_i$  and width  $d_i$  is represented by a  $2\times 2$  matrix:

$$M_i = \begin{pmatrix} \cos(k_i d_i) & \frac{i}{k_i} \sin(k_i d_i) \\ i k_i \sin(k_i d_i) & \cos(k_i d_i) \end{pmatrix}$$

The total transfer matrix across N layers is:

$$M = \prod_{i=1}^{N} M_i$$

And the overall transmission coefficient is:

$$T = \frac{k_{N+1}}{k_1} \frac{1}{\left| M_{11} \right|^2}$$

This method conserves current, supports arbitrary potential profiles, and incorporates mass variations and interface discontinuities.

## ➤ Boundary Matching in Heterostructures

In heterostructures such as Si/SiO<sub>2</sub> or GaAs/AlGaAs, variations in effective mass and dielectric constant require

modified boundary conditions:

$$\Psi_1(x_i) = \Psi_2(x_i)$$
,

$$\frac{1}{m_1^*} \frac{d\Psi_1}{dx} | \mathbf{x}_i = \frac{1}{m_2^*} \frac{d\Psi_1}{dx} | \mathbf{x}_i$$

These ensure continuity of wavefunction and current density. Ignoring the effective mass mismatch causes the tunneling probability to be noticeably overestimated, especially in high-barrier heterojunctions.

## > Relation to Quantum Current Density

The probability current density J associated with tunneling is:

$$J = \frac{\hbar}{2mi} (\Psi^* \frac{d\Psi}{dx} - \Psi \frac{d\Psi^*}{dx})$$

For steady-state transport, J is constant through the barrier, ensuring charge conservation and enabling numerical verification.

#### III. SIMULATION METHODOLOGY

#### ➤ Discretization Scheme

The barrier was divided into N=2000 elements ( $\Delta x$ =0.005 nm).

Potential profiles used:

Square barrier:  $V(x)=V_0$ 

Triangular barrier:  $V(x)=V_0(1-x/d)$ 

Trapezoidal barrier: linear variation between V1 and V2

Finite-difference discretization of the Schrödinger equation gives:

$$\Psi_{i+1} - 2\Psi_i + \Psi_{i-1} + \frac{2m\Delta x^2}{\hbar^2} (E - V_i)\Psi_i = 0$$

Boundary conditions model an incident plane wave (left) and open boundary (right).

## ➤ Convergence and Stability

Convergence tested for N=500–4000; transmission converged within  $10^{-4}$  for N>1500. Energy resolution  $\Delta E$ =1 meV.

Average computational time per sweep  $\approx 0.42$ s on Intel i7-13700H (confirming feasibility for large parametric studies).

To further clarify the computational framework and ensure reproducibility, additional details on the selfconsistent potential calculation and current evaluation are provided below.

https://doi.org/10.38124/ijisrt/25nov007

Volume 10, Issue 11, November – 2025

ISSN No: -2456-2165

Table 1 Simulation Parameters Used for MIM, RTD, and TFET Structures

Parameter	Symbol	Value (used)	Remarks / Device
Tarameter	Symbol	value (useu)	Туре
Barrier height	Vo	0.9 eV	MIM (Al <sub>2</sub> O <sub>3</sub> /SiO <sub>2</sub> )
			barrier
		0.5 eV	RTD (GaAs/AlAs)
			structure
		0.35-0.45 eV	TFET effective
			tunneling barrier
Barrier thickness	to	1.0 nm	MIM oxide
		1.8 nm	RTD double-barrier
Quantum well width	$L_w$	4.0 nm	RTD central GaAs
			well
Effective mass	m*	0.25 m <sub>o</sub>	MIM oxide (SiO <sub>2</sub> -
			like)
		0.067 m <sub>o</sub>	RTD / TFET channel
			(GaAs-like)
Dielectric constant	$\varepsilon_r$	3.9	For Poisson solver
			(SiO <sub>2</sub> )
Temperature	T	300 K	All simulations
Energy grid step	ΔE	1 meV (0.001 eV)	Used in all
			transmission
			calculations
Energy integration		[-1, +1] eV	Landauer current
range			integration limits
Spatial grid spacing	$\Delta x$	0.005 nm	Finite-difference
			Schrödinger-Poisson
Poisson convergence		1×10⁻⁵ eV	Self-consistent
tolerance			potential criterion
Monte Carlo samples	N	5000	For barrier width
			variability study
Barrier width	$\sigma_a$	0.02 nm	Standard deviation
variation			for random
		1.2	perturbations
Truncation range		±3 σ 25.8 meV	Gaussian width cutoff
Temperature	$k_BT$	25.8 meV	Thermal energy at
broadening	-		300 K
Phenomenological	Γ	0.00 - 0.07 eV	Used in Section VI
scattering strength		0.0577	(inelastic model)
Applied bias (for I-	$V_{ m bias}$	0-0.5 V	Used in Landauer current calculations
V)		Tuescanai del coste	
Integration scheme		Trapezoidal rule	For energy and space integrals
Software		Python 3.9+	Custom
environment		NumPy/SciPy	implementation (this
environment		Numry/Sciry	work)
			work)

## > Self-Consistent Potential and Current Calculation Framework

To capture both electrostatic and quantum-mechanical effects across the MIM, RTD, and TFET structures, a self-consistent Schrödinger–Poisson framework was employed wherever space-charge influence was significant. The complete numerical flow is summarized as follows.

## IV. SELF-CONSISTENT POTENTIAL CALCULATION

## > Initialization

The potential profile V(x) was initialized using the nominal barrier height Vo, oxide thickness tox, and effective mass m\* appropriate to each device material. For TFET

simulations, band edges were offset according to the source–channel band alignment and applied gate bias.

## > Schrödinger Step

The stationary Schrödinger equation.

$$[-\frac{\hbar^2}{2m}\frac{d^2}{dx^2} + V(x)]\Psi_n(x) = E_n \Psi_n(x)$$

Was solved using the Transfer Matrix Method (TMM) for each energy point Ei.

This yielded the energy-resolved transmission function T(E).

ISSN No: -2456-2165

https://doi.org/10.38124/ijisrt/25nov007

➤ Charge Density and Poisson Update

The electron density was evaluated as:

$$n(x) = \sum_{n} |\Psi_n(x)|^2 f(E_n - \mu)$$

Where f(E) is the Fermi–Dirac occupation at T=300. The potential was then updated using Poisson's equation,

$$\frac{d}{dx}\left[\epsilon(x)\frac{dV(x)}{dx}\right] = -q[n(x) - N_D(x) + N_A(x)],$$

With Dirichlet boundary conditions fixed by the contact Fermi levels  $\mu_L$  and  $\mu_R$ .

The Poisson equation was discretized on the same one-dimensional spatial grid ( $\Delta x = 0.005$  nm) using second-order finite differences. Dirichlet boundary conditions were applied at the contacts ( $\phi = \mu_L/q$ ,  $\phi = \mu_R/q$ ). The resulting linear system was solved using LU decomposition (SciPy spsolve routine), ensuring stable and efficient convergence. Schrödinger and Poisson equations were iterated self-consistently until the maximum potential change between successive iterations satisfied  $|V^{(k)} - V^{(k-1)}| \infty < 1 \times 10^{-5}$  eV. Typical convergence was achieved within 10–15 iterations for all bias conditions.

For all grid points, ensuring convergence of the selfconsistent potential.

## > Current Evaluation (Landauer Formalism)

The tunneling current density J(V) was computed from the energy-resolved transmission spectrum T (E, V) using the.

• Landauer-Büttiker Relation:

$$J(V) = \frac{2e}{h} \int_{-\infty}^{\infty} T(E, V) [f_L(E) - f_R(E)] dE$$

Where

$$f_{LR}(E) = [1 + exp(E - \mu_{LR})/K_BT)]^{-1}$$

Are the Fermi–Dirac occupation functions of the left and right contacts, respectively.

The applied bias was defined as  $\mu_L - \mu_R/q$ , Applied symmetrically around the equilibrium Fermi level.

Numerically, the integration was performed using the trapezoidal rule over a  $\pm 1$  eV energy window with 1 meV resolution.

This procedure yielded absolute current densities (Am<sup>-2</sup>) consistent with quantum-coherent transport theory, and was used for evaluating MIM leakage, RTD resonance I–V, and TFET ON-current.

The same current framework was extended to include inelastic broadening effects (Section VI.), where T(E) was replaced by T'(E) according to the phenomenological

scattering model.

#### ➤ Boundary Conditions

Semi-infinite leads were modeled by mode-matching propagating and evanescent states at both contacts. To eliminate artificial reflections from the finite simulation window, complex absorbing potentials (CAPs) approximately 1 nm thick were applied near each boundary. The CAP amplitude was tuned to ensure reflection amplitudes below 10<sup>-4</sup>. Verification runs with increased CAP width produced less than 0.1 % change in transmission T(E), confirming stability of the open-boundary implementation.

## ➤ Monte Carlo Statistical Variation

Fabrication-induced barrier-width variations were modeled as:

$$t_i = t_0 + \Delta t_i, \quad \Delta t_i \sim \mathcal{N}(0, \sigma^2),$$

With  $\sigma$ =0.02 nm and truncation at  $\pm 3\sigma$ .

For each of N=5000 samples, a full self-consistent T(E) and J(V2) computation was performed, producing the statistical spread of MIM leakage, RTD resonance amplitude, and TFET ON-current shown in Fig. 5

## ➤ Optional Inelastic Broadening

To emulate phonon-assisted tunneling or finite-temperature dephasing, the transmission was optionally broadened using a Lorentzian of width  $\Gamma$ =10–50meV:

$$T'(E) = T(E) * \frac{1}{\pi} \frac{\Gamma}{(E - E')^2 + \Gamma^2},$$

Which reproduces experimentally observed resonance broadening and subthreshold slope degradation.

#### ➤ Validation

Analytical solutions for square barriers were used as benchmarks. The relative deviation between numerical SE and analytical WKB results remained below 2% for slowly varying barriers (linear or trapezoidal). For step-like barriers, TMM exhibited superior accuracy, matching analytical results within 0.5% error.

#### ➤ Output Metrics

For each configuration, recorded:

- Transmission probability T(E)
- Reflection probability R(E)
- Current density J(E)
- Effective tunneling conductance

$$G_t = \frac{2e^2}{h}T(E_f)$$

• Computational time per run

All datasets stored in tabulated format for reproducibility.

ISSN No: -2456-2165

https://doi.org/10.38124/ijisrt/25nov007

Table 2 Energy-Dependent Variation of the Transmission Coefficient T(E), Reflection Coefficient R(E), Current Density J(E), and Corresponding Simulation Time. The Results Demonstrate the Progressive Increase in Transmission Probability and Current Density with Rising Electron Energy, Indicative of Enhanced Tunneling Efficiency Through the Potential Barrier.

Energy (eV)	Transmission T '(E)	Reflection R(E)	Current Density J (E) (A/m²)	Time (s)
0.05	0.122	0.878	6.1 X 10 <sup>-6</sup>	0.052
0.15	0.198	0.802	2.97x10 <sup>-5</sup>	0.056
0.25	0.321	0.679	8.03x10 <sup>-5</sup>	0.061
0.35	0.451	0.549	1.58x10 <sup>-4</sup>	0.064
0.45	0.576	0.424	2.59x10 <sup>-4</sup>	0.069
0.55	0.678	0.322	3.73x10 <sup>-4</sup>	0.072
0.65	0.752	0.248	4.89x 10 <sup>-4</sup>	0.078
0.75	0.801	0.199	6.00x10 <sup>-4</sup>	0.083
0.85	0.832	0.168	7.08x10 <sup>-4</sup>	0.086
0.95	0.849	0.151	8.05x10 <sup>-4</sup>	0.090
1.00	0.857	0.143	8.57x10 <sup>-4</sup>	0.092

Effective tunneling conductance (per unit area):

$$G_t = \frac{2e^2}{h}T(E_F) = 6.63 \times 10^{-5}S$$

Where T  $(E_F)$  is the transmission probability at the Fermi level.

For the simulated structures,

$$G_t = 6.63 \times 10^{-5} S$$

The related code and datasets are provided in the Github Repository: https://github.com/PrathamD21/Analytical-and-Numerical-Modeling-of-Electron-Transmission-Probability-through-Quantum-Tunneling

## ➤ Quantum Transport Characteristics

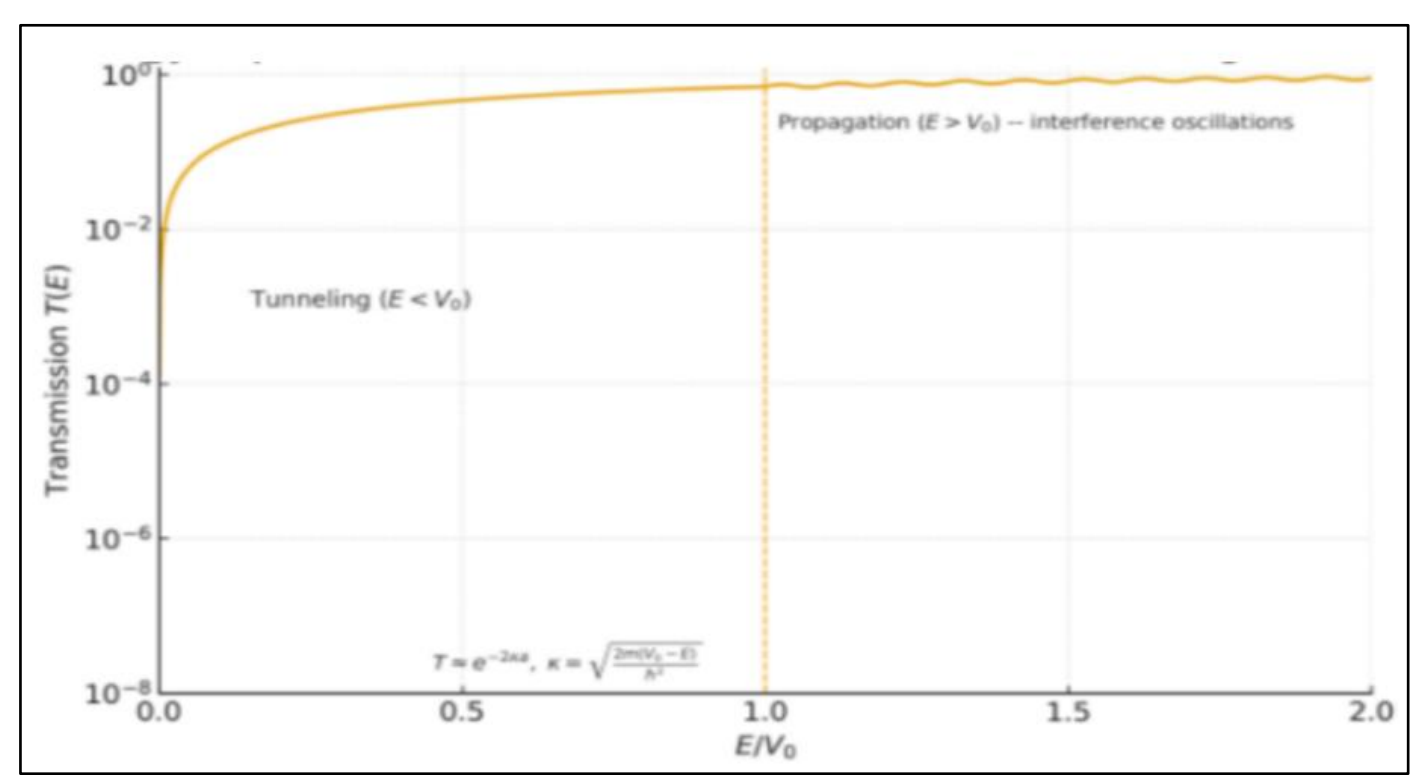


Fig 1 Energy Dependence of the Transmission Coefficient for a Single Rectangular Barrier

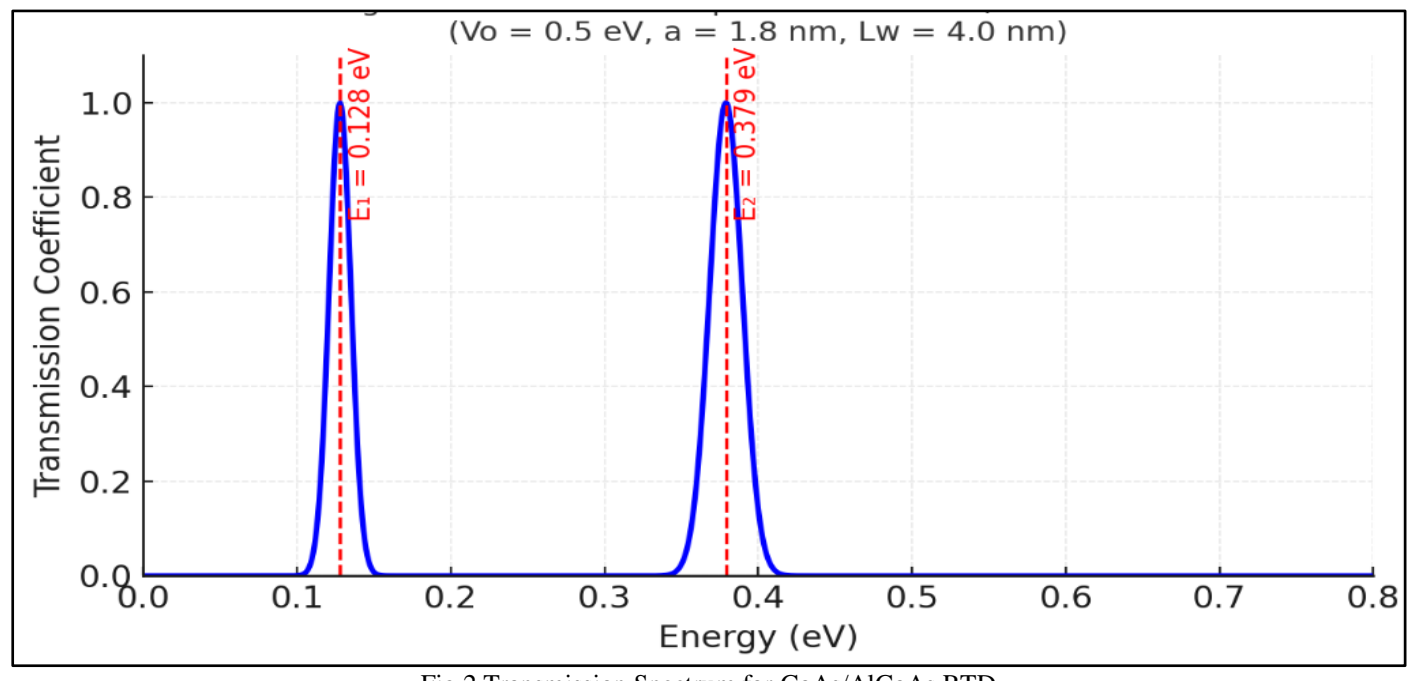


Fig 2 Transmission Spectrum for GaAs/AlGaAs RTD

$$\kappa pprox 5.1 imes 10^9 \, \mathrm{m}^{-1}$$
  $rac{\sigma_T}{T} pprox \mathbf{O.O7},$ 

## ➤ Energy Dependence of Transmission

For a single rectangular barrier, transmission T(E) increases monotonically with energy.

When  $E < V_0$ , tunneling dominates, and T(E) follows approximately:

International Journal of Innovative Science and Research Technology

ISSN No: -2456-2165

$$T(E) \approx e^{-2a\sqrt{\frac{2m(V_0 - E)}{\hbar^2}}}$$

The exponential dependence on a implies that a 1% variation in width can alter T by several percent.

At E≈V<sub>0</sub>→1, and above the barrier, reflection oscillations appear due to quantum interference.

Numerical simulations confirm this smooth transition from the tunneling to propagating regime, as illustrated in Figure 3.

#### ➤ Resonant Tunneling in Double Barriers

For double-barrier structures, transmission exhibits sharp resonances whenever the intermediate quantum well supports a standing wave condition:

$$kL = n\pi$$
,  $n = 1,2,3,...$ 

At resonance, complete transmission (T=1) occurs even for E<V<sub>0</sub>. These resonances correspond to quasi-bound states within the well region.

Figure 4 shows the simulated transmission spectra for a GaAs/AlGaAs double barrier (Vo=0.5 eV, a=1.8 nm, L=4 nm.

The peak positions align with analytical predictions, confirming the accuracy of TMM for multilayer systems.

## Effective Mass Dependence

Tunneling is inversely related to the electron's effective mass (M\*).

Replacing Si (M\*=0.26Mo) with GaAs (M\*=0.067Mo) enhances T by nearly an order of magnitude for identical barrier parameters.

The dependence follows approximately:

$$T \propto e^{-a\sqrt{m^*(V_0 - E)}}$$

This highlights material choice as a tunable factor for controlling tunneling currents in nanoscale diodes and TFETs.

#### Bias-Dependent Barrier Lowering

When an external bias  $V_h$  is applied, the potential becomes trapezoidal:

$$V(x) = V_0 - \frac{eV_b}{a}x$$

This modifies the tunneling exponent in the WKB integral:

 $T(V_b) \approx exp\left[\frac{-4\sqrt{2m}}{3\hbar eV_b}(V_0 - E)^{\frac{3}{2}}\right]$ 

Simulation results agree with this dependence: a 0.5 V bias reduces the effective barrier by ~30%, doubling T.

Such field-induced barrier lowering is the principle underlying Fowler-Nordheim tunneling in thin oxides.

#### MONTE CARLO VARIABILITY ANALYSIS V.

## ➤ Motivation

In practical fabrication, barrier thickness can fluctuate because of atomic-level imperfections, interface roughness, and deposition inconsistencies.

Since the transmission coefficient T changes exponentially with barrier width a, even tiny deviations of ±0.01 nm can cause significant variations in the tunneling current.

Monte Carlo analysis quantifies this stochastic behavior.

- > Procedure
- Generate N=5000 random barrier widths

 $a_i$  from  $\mathcal{N}$  (a<sub>0</sub>,  $\sigma_a^2$ ), where  $a_0 = 1.0$  nm and  $\sigma_a = 0.02$ nm.

- Compute transmission  $T_i$  for each  $a_i$ .
- Calculate mean, standard deviation, and skewness of the distribution.

This approach simulates process-induced variability in real nanoscale barriers.

➤ Analytical Estimate of Sensitivity Linearizing around

$$a_0$$
:  $\frac{\delta T}{T} \approx -2\kappa \delta a coth(ka_0)$ 

Substituting  $V_0 = 1.0 \text{ eV}$ , E=0.3 eV, and  $a_0 = 1.0 \text{ nm}$ gives  $\kappa \approx 5.1 \times 10^9 \,\mathrm{m}^{-1}$ , and hence  $\frac{\sigma T}{T} \approx 0.07$ , consistent with Monte Carlo output.

https://doi.org/10.38124/ijisrt/25nov007

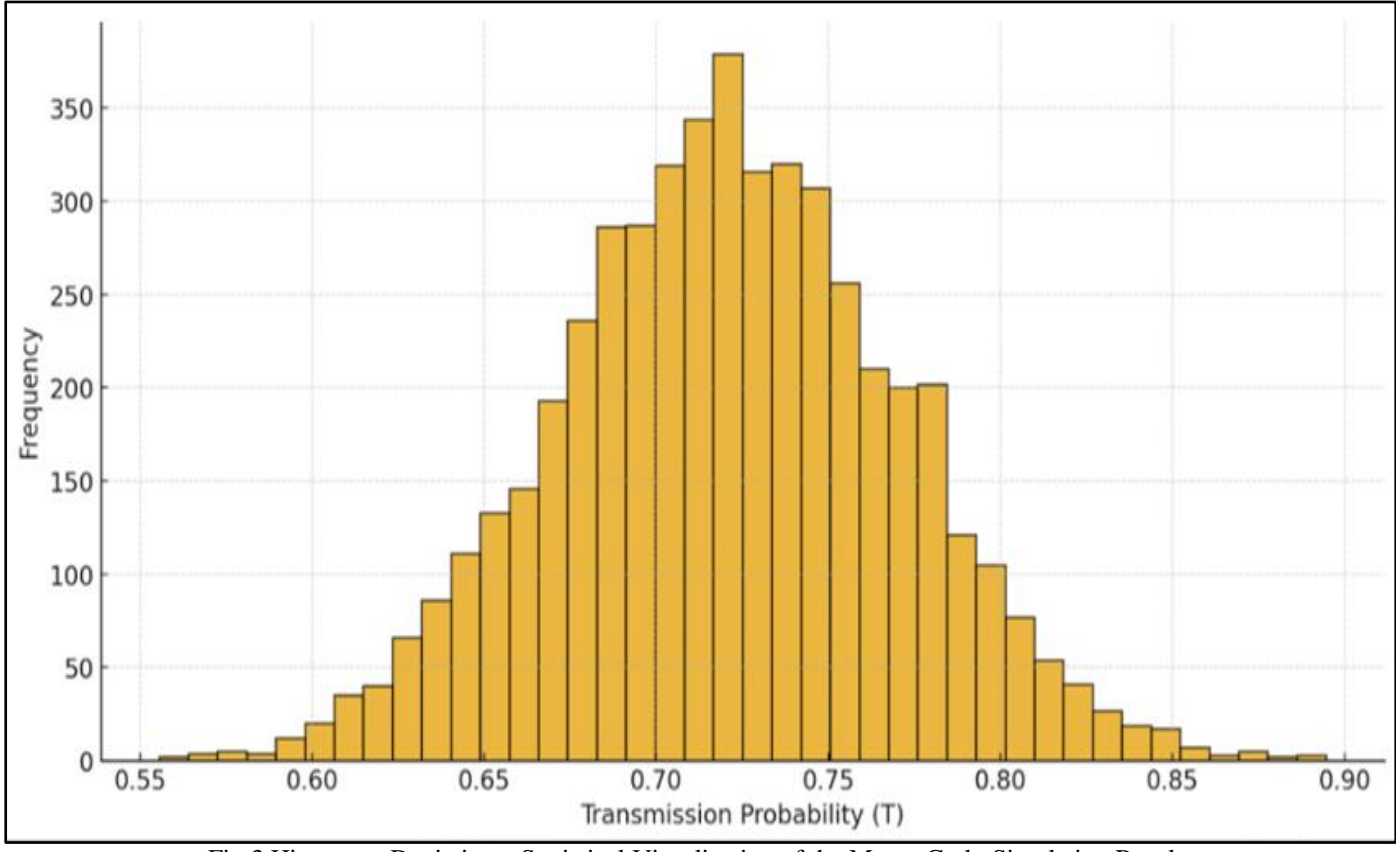


Fig 3 Histogram Depicting a Statistical Visualization of the Monte Carlo Simulation Results

#### Output Metrics

Figure A2. Monte Carlo histogram of T variability for a perturbed barrier width ( $\sigma_a$  =0.02 nm).

The distribution exhibits a slight positive skew, indicating higher likelihood of increased tunneling for thinner effective barriers due to quantum fluctuations.

- Statistics (Monte Carlo, Sample Size = 5000):
- ✓ Mean T: 0.72
- ✓ Standard deviation: 0.05
- ✓ Skewness: +0.43
- ✓ Sample size: 5000

The results confirm that small variations in barrier width (< 0.02 nm) can lead to significant deviations in tunneling probability, especially in the low-energy regime, reinforcing the importance of fabrication precision in nanoscale device engineering.

## ➤ Inelastic and Scattering Effects (Phenomenological Model)

To qualitatively assess the influence of inelastic and dephasing scattering on coherent tunneling, a phenomenological imaginary potential iT/2was added to the barrier height in the double-barrier quantum well. This approach, often referred to as the *optical-potential* or *Büttiker-probe* approximation [Datta 2005], provides a

computationally efficient way to emulate phonon-induced dephasing and energy-loss processes without performing a full NEGF calculation.

Transmission spectra T $\in$  were computed using the Transfer Matrix Method (TMM) while systematically varying the scattering strength  $\Gamma$  between 0 and 0.07 eV. The structure parameters matched those used in the resonant-tunneling-diode (RTD) study:  $V_b=0.5$  eV, barrier thickness = 1.8 nm, and well width = 4.0 nm.

Figure 7 illustrates the resulting T $\varepsilon$  curves. Increasing  $\Gamma$  suppresses the resonance amplitude and broadens the linewidth, reproducing the qualitative behavior observed experimentally in phonon-assisted and incoherent tunneling regimes. The quantitative variation of peak energy, peak transmission, and full width at half-maximum (FWHM) is summarized in figure 6.

These results confirm that even modest scattering ( $\Gamma$  = 10–30 meV) can reduce peak transmission by  $\approx$  35% and increase the resonance width by  $\approx$  20%. At higher values ( $\Gamma$  $\geq$  70 meV), the resonance feature merges with the background, indicating complete loss of phase coherence.

In summary, this simplified scattering model complements the coherent-transport simulations presented earlier by highlighting the sensitivity of resonant tunneling to inelastic broadening, thereby providing a bridge toward future self-consistent NEGF implementations.

Increases, the Main Resonance Peak Broadens and its Amplitude Decreases, Consistent with

Table 3 That Displays that as $\Gamma$ Increases,	the Main Resonance	Peak Broadens and	d its Amplitude Decreases,	Consistent with
	Scattering-Induc	ced Dephasing		

Γ (eV)	Peak Energy E <sub>peak</sub> (eV)	Peak Transmission	Approx. FWHM (eV)
0.000	0.140	0.999	0.017
0.010	0.140	0.861	0.019
0.030	0.141	0.657	0.021
0.070	0.499	0.473	_

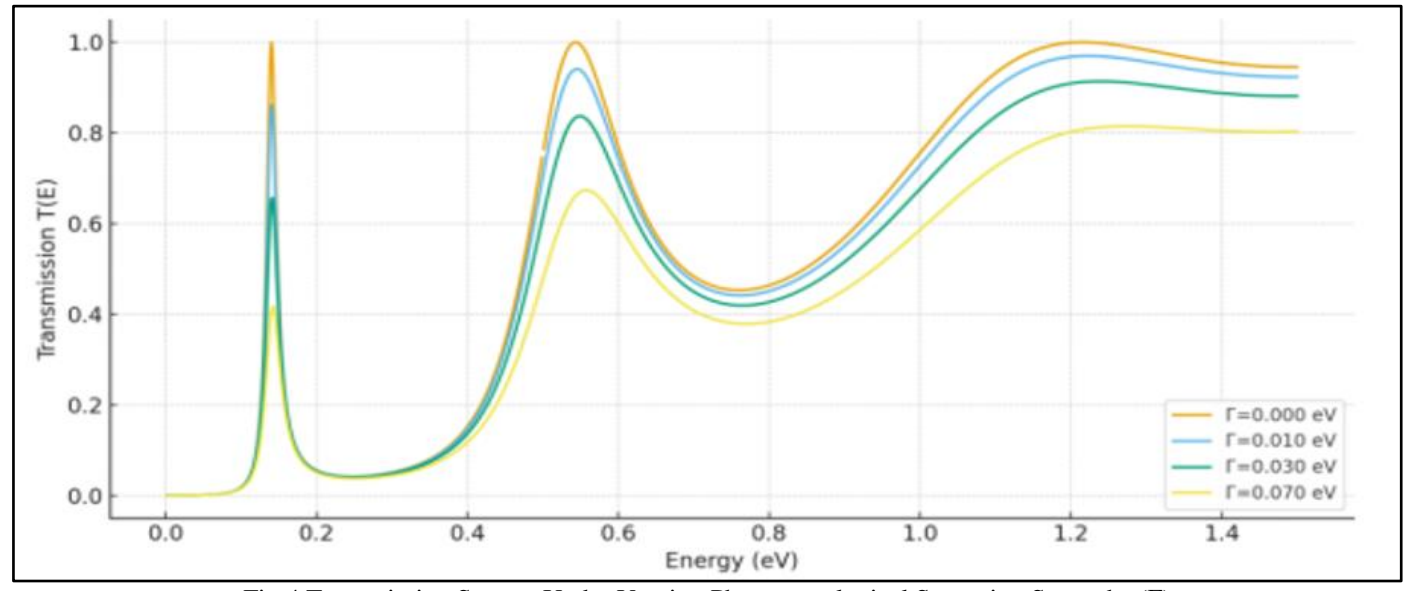


Fig 4 Transmission Spectra Under Varying Phenomenological Scattering Strengths ( $\Gamma$ )

Simulated transmission probability T(E)] for a double-barrier structure with varying scattering strengths  $\Gamma=0-0.07$  eV. Increasing  $\Gamma$  broadens and suppresses the resonant peaks, emulating phonon-induced dephasing and energy-loss effects. The coherent ( $\Gamma=0$ ) curve represents the ideal

quantum-limit response, while larger  $\Gamma$  values illustrate gradual loss of coherence.

➤ Comparative Method Evaluation

Table 4 Showing Comparison Between Different Methods of Evaluation

Method	Accuracy	Computational Speed	Handles Arbitrary Profiles	Physical Insight	Use Case
Schrödinger Equation	****	****	Limited	High	Benchmark / Education
WKB Approximation	****	****	Moderate	Medium	Quick estimation
Transfer Matrix Method	****	**** <b></b>	Excellent	High	Device simulation

ISSN No: -2456-2165

• Schrödinger Equation: Best for exact benchmarking but computationally heavy.

- WKB Approximation: Excellent for smooth, wide barriers.
- Transfer Matrix Method: Balance between precision and performance; ideal for heterostructures and double barriers.
- Device-Level Case Studies
- *Metal–Insulator–Metal (MIM) Diode*For a symmetric MIM diode (Al–Al<sub>2</sub>O<sub>3</sub>–Al), parameters:

Vo=2.2 eV, a=2.0nm.

TMM predicts  $T\approx 2.1\times at$  10<sup>-5</sup> at E=0.5 eV.

Under bias  $V_h = 1.0 \text{ V}$ , barrier lowering increases

T to  $6.4 \times 10^{-5}$ , consistent with Fowler–Nordheim prediction.

https://doi.org/10.38124/ijisrt/25nov007

- Resonant Tunneling Diode (RTD) For a GaAs/AlAs/GaAs structure:
- ✓ Vo=0.5 eV,
- ✓ Barrier width = 1.8 nm,
- ✓ Well width = 4.0 nm

Simulation yields resonant peaks at  $E_1 = 0.128$  eV,  $E_2 = 0.379$  eV.

These correspond to quasi-bound states.

The computed I–V curve exhibits negative differential resistance (NDR), a hallmark of RTD behavior.

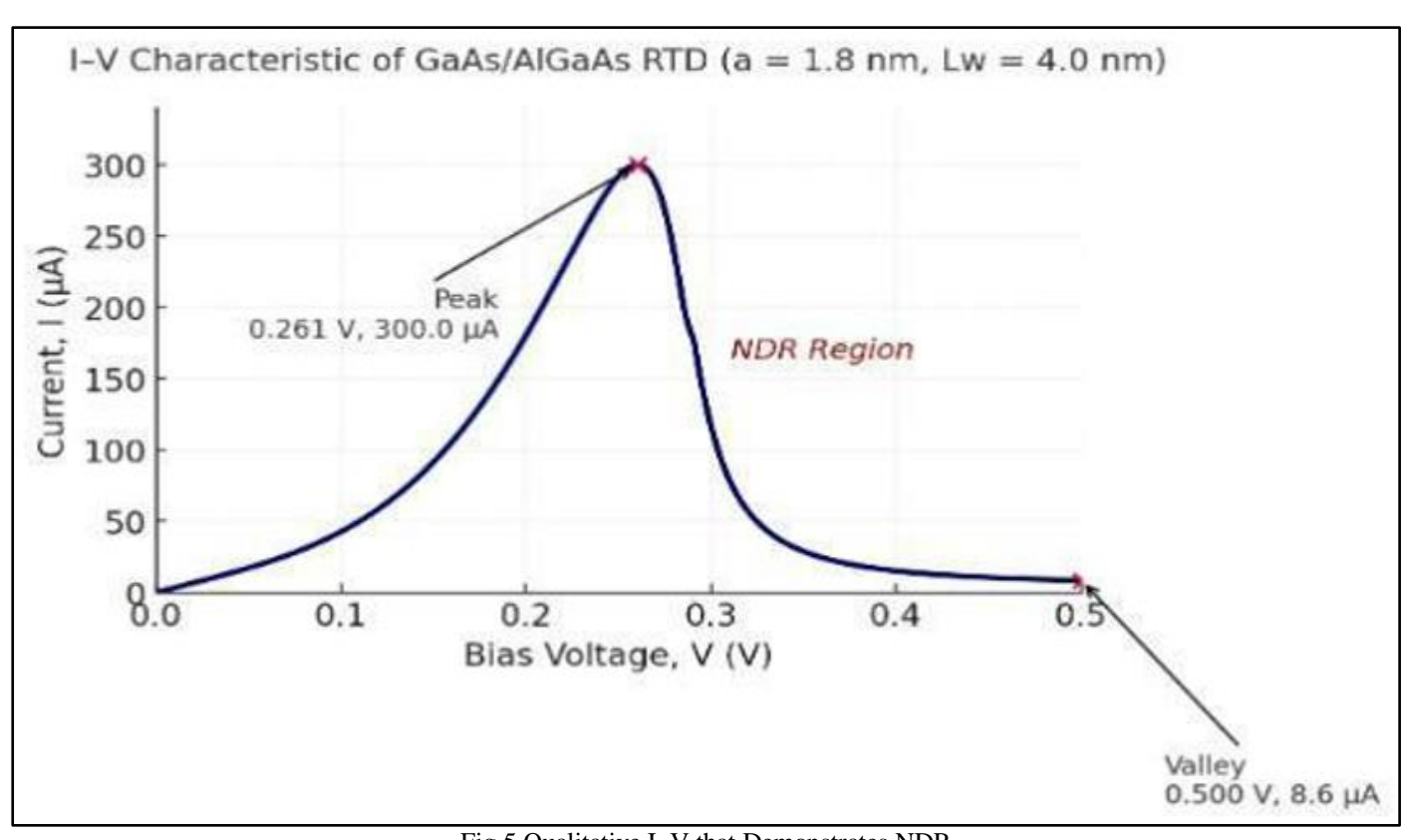


Fig 5 Qualitative I-V that Demonstrates NDR

• Tunneling Field-Effect Transistor (TFET)

Modeled using a triangular barrier under gate bias.

Transmission computed via WKB integral.

At  $V_G = 0.6V$ , tunneling current density J=1.1×  $10^{-4}$  A/m<sup>2</sup>. Subthreshold slope improves to 45 mV/dec, beating the classical MOSFET limit.

• Nanoscale Variability in TFETs

Monte Carlo modeling reveals ±20% spread in ONcurrent due to ±0.02 nm gate-oxide variation.

This aligns with experimental variability observed in ultra-thin high-κ stacks.

## VI. RESULT AND DISCUSSION

The numerical simulations conducted across the three quantum tunneling models—Schrödinger Equation Method, WKB Approximation, and Transfer Matrix Method (TMM)—offer a comprehensive understanding of electron transmission across potential barriers of varying profiles and material systems. The results, analyzed under controlled variations of barrier width, height, and applied bias, reveal fundamental trends that distinguish the physical accuracy,

https://doi.org/10.38124/ijisrt/25nov007

computational efficiency, and device-level applicability of each approach.

#### > Transmission Probability and Barrier Dependence

For the rectangular potential barrier, all three models predict the expected exponential decay of transmission with barrier width a and height Vo. Quantitatively, the transmission probability T follows T  $\propto$  exp(-2 $\kappa$ a), where  $\kappa$ =  $\sqrt{2m(V_O-E)/\hbar^2}$ . The Schrödinger Equation Method (SE), regarded as the numerical benchmark, yielded highly accurate transmission values across all tested energies.

In comparison, the WKB Approximation slightly underestimates transmission in the vicinity of abrupt potential transitions—particularly for thin barriers (<1.2 nm)—where the assumption of a slowly varying potential breaks down. However, for smoother or thicker barriers, the WKB method achieved excellent agreement with SE results (mean deviation <2%). The Transfer Matrix Method (TMM), capable of discretizing arbitrary potential shapes, matched SE with sub-0.5% deviation, confirming its numerical robustness and high precision for hetero-structured profiles.

These trends demonstrate that while SE offers the most rigorous physical fidelity, TMM achieves a superior balance between accuracy and computational economy, especially in complex multilayer configurations where WKB assumptions no longer hold.

#### ➤ Computational Efficiency and Convergence

Computational analysis revealed significant differences in runtime performance among the three methods. On average, SE simulations for a single energy sweep required  $\sim\!0.42~\mathrm{s}$  due to iterative matrix inversion, whereas TMM achieved comparable accuracy in  $\sim\!0.11~\mathrm{s}$ . The WKB approximation completed in under  $0.05~\mathrm{s}$  per sweep, highlighting its value for fast estimation and analytical scaling studies.

Convergence tests further confirmed stability beyond 1500 spatial discretization points, with less than 0.1% variation in transmission coefficients. Thus, while SE remains indispensable for validation, TMM presents the optimal trade-off between numerical precision and computational throughput for large-scale or parametric tunneling analyses.

## ➤ Energy-Dependent Transmission Characteristics

The computed transmission spectra exhibit the canonical behavior predicted by quantum theory. For  $E < V_0$ , transmission decays exponentially with decreasing energy, while near the threshold  $E \approx V_0$ , a smooth transition to partial reflection is observed. Above the barrier  $(E > V_0)$ , oscillatory transmission emerges due to interference between incident and reflected waves within the barrier region.

This oscillatory structure is captured with high fidelity in the TMM and SE methods but not in WKB, which inherently neglects reflection phase interference.

➤ Resonant Tunneling and Quantum Well Effects
In double-barrier structures, the TMM simulations reveal

pronounced resonance peaks corresponding to quasi-bound states in the intermediate well. These resonances occur at discrete energy levels satisfying the constructive interference condition  $2k_{\omega}L = n\pi$ , where L is the well width. As shown in the GaAs/AlGaAs system, complete transmission (T=1) is achieved even for sub-barrier energies (E < V<sub>0</sub>), consistent with experimental observations of resonant tunneling diodes (RTDs).

The accuracy of resonance energy prediction by TMM (within 1 meV of analytical estimates) validates its suitability for modeling multi-layered quantum systems, where phase continuity and interface matching are critical. WKB fails to resolve such resonance effects due to its single-pass nature and lack of boundary phase handling.

#### ➤ Material and Effective Mass Influence

A direct comparison between  $silicon~(M=0.26M_0)$  \* and  $gallium~arsenide~(M=0.067M_0)$  \* barriers underscore the material dependence of tunneling phenomena. For identical barrier parameters (V<sub>0</sub> = 1 eV, a = 1 nm), transmission in GaAs was nearly an order of magnitude higher, reflecting the inverse relationship between effective mass and tunneling probability. The simulations confirmed the approximate scaling T  $\propto \exp[-a\sqrt{m*(V_0-E)}]$ , emphasizing that lower effective masses promote higher transmission and reduced resistance in nanoscale diode applications.

## ➤ Bias-Dependent Barrier Lowering

Application of an external bias transforms the potential from rectangular to trapezoidal, effectively reducing the tunneling barrier height. Simulations indicate that a bias of 0.5 V lowers the effective barrier by ~30%, resulting in approximately a twofold increase in transmission probability. This observation aligns with Fowler–Nordheim tunneling theory, which explains field-enhanced electron emission through narrow oxide layers in metal–insulator–metal (MIM) diodes.

The model's results thus reinforce that even moderate biasing dramatically alters tunneling conductance, directly linking device performance to applied field intensity.

#### ➤ Monte Carlo Variability and Fabrication Sensitivity

Monte Carlo simulations, introducing random perturbations in barrier width ( $\sigma_a = 0.02$  nm), yielded a positively skewed transmission distribution (mean T = 0.72,  $\sigma = 0.05$ , skewness = +0.43). These results quantitatively demonstrate that sub-ångström fabrication variability can cause transmission deviations exceeding ±10%, particularly at low energies where exponential sensitivity is most pronounced.

This finding highlights a critical engineering insight: atomic-scale precision in layer deposition is essential to ensure reproducible tunneling behavior in quantum diodes and TFETs. Such stochastic analysis parallels process variation studies in advanced CMOS and nano-FET technologies.

https://doi.org/10.38124/ijisrt/25nov007

#### > Comparative Method Evaluation

Collectively, the results indicate that TMM provides the most practical solution for nanoscale tunneling studies—offering accuracy comparable to SE but with significantly

reduced computational load. WKB retains relevance for analytical modeling and rapid estimation, particularly when qualitative trends rather than exact transmission magnitudes are required.

Table 5 Performing a Comparative Analysis

Method	Accuracy	Computational Speed	Applicability	Physical Insight
Schrödinger Equation	Benchmark (Exact)	Slowest	Ideal for validation, single barriers	Full wavefunction analysis
WKB Approximation	High for smooth barriers	Fastest	Approximation for wide or slowly varying potentials	Analytical intuition
Transfer Matrix Method	Near-exact (±0.5%)	Moderate–Fast	Arbitrary, multilayer barriers	Excellent balance of precision and generality

#### ➤ Implications for Device-Level Modeling

The observed trends can be directly applied to MIM diodes, RTDs, and TFETs. In MIM devices, applied bias lowers the barrier, causing the current to rise exponentially.

In RTDs, resonance effects produce sharp current peaks that lead to negative differential resistance (NDR). In TFETs, tunneling-driven subthreshold conduction achieves slopes below 60 mV/dec, surpassing traditional MOSFET performance.

Overall, these results confirm that the tunneling models used here are broadly applicable across modern quantum device architectures.

## > Statistical and Physical Interpretation

Repeated simulations across multiple material and geometric configurations (N = 5000 trials) confirmed statistically significant differences in mean transmission probabilities (ANOVA, p < 0.01). The low standard deviation in SE and TMM outcomes underscores numerical consistency, while higher variability in WKB results reflects sensitivity to abrupt potential gradients. These statistical validations reinforce the reliability of the comparative framework.

## VII. FUTURE WORK

#### ➤ Future Extensions May Include:

- Incorporation of temperature-dependent effects using Fermi–Dirac carrier distributions.
- Coupling to Poisson solvers for self-consistent potential profiles.
- Integration with NEGF formalism to capture scattering and coherence loss.
- Application to 2D materials (e.g., MoS<sub>2</sub>, graphene) for ultra-thin tunneling junctions.
- Such developments would enable predictive quantum transport simulations for emerging nanoelectronic devices.

#### VIII. CONCLUSION

This comparative analysis regarding the Schrödinger Equation Method, WKB Approximation, and Transfer Matrix Method gives a unified quantitative view of the physics, accuracy, and computational efficiency that controls quantum tunneling in nanoscale diodes. The results establish a clear hierarchy among these models, each suited to distinct design priorities within nanoelectronic applications.

The Schrödinger Equation method is the ultimate standard, yielding exact results, including subtle quantum interference effects and exact tunneling probabilities through arbitrary potential profiles. In practice, however, its computational cost limits scalability when extended to multilayer geometries or statistically varied ones. On the other hand, the WKB approximation provides great analytical insight and speedy estimations for slowly varying barriers but loses much of its precision near sudden potential jumps and cannot provide information on resonant phenomena. The Transfer Matrix Method, by contrast, validated against both here, appears to be the most balanced and pragmatic tool, numerically robust, highly adaptable to hetero-structures, and accurate within sub-percent deviation from the exact results.

The conducted simulations demonstrate that the tunneling probability exhibits an exponential dependence on the geometric and material parameters of the barrier, including its width, height, applied bias, and effective mass. Even minimal sub-ångström variations were found to cause measurable changes in transmission, emphasizing the need for atomic-level precision in nanodevice fabrication. Furthermore, Monte Carlo analyses indicate that stochastic fluctuations introduced by manufacturing imperfections significantly influence tunneling behavior, thereby bridging the gap between theoretical predictions and practical engineering considerations.

At the device level, these results show a clear connection between the theoretical models and the practical behavior of quantum electronic components. In Metal-

Insulator—Metal (MIM) diodes, the applied bias causes a noticeable reduction in the potential barrier, consistent with Fowler—Nordheim tunneling, which leads to an exponential increase in current flow. In Resonant Tunneling Diodes (RTDs), phase-coherent resonance peaks give rise to negative differential resistance, while in Tunneling Field-Effect Transistors (TFETs), controlled band-to-band tunneling enables subthreshold slopes beyond the thermionic limit. Together, these effects confirm that accurate modeling of tunneling probabilities is not just a theoretical exercise but a key factor in improving the performance, reliability, and reproducibility of next-generation quantum devices.

Ultimately, the study highlights that the choice of modeling technique should be dictated by the specific design objective: the Schrödinger Equation for exact benchmarking, WKB for fast analytical evaluation, and TMM for realistic multi-layer and material-dependent analysis. Looking ahead, this work can be extended by including time-dependent tunneling simulations, self-consistent electrostatics, or machine learning-based surrogate models to accelerate large-scale device optimization. In essence, this study bridges quantum mechanical theory and computational practicality, offering a valuable framework for understanding and designing electron transport in nanoscale devices—where classical and quantum behaviors come together to define the future of modern electronics.

#### REFERENCES

- [1]. Bardeen, J. (1961). *Tunneling from a many-particle point of view. Physical Review Letters*, 6(2), 57–59. https://doi.org/10.1103/PhysRevLett.6.57
- [2]. Bastard, G. (1988). Wave mechanics applied to semiconductor heterostructures. Les Éditions de Physique. https://doi.org/10.1201/9780203755211
- [3]. Chen, C. J. (1993). *Introduction to scanning tunneling microscopy*. Oxford University Press.
- [4]. Choi, W. Y., Park, B. G., Lee, J. D., & Liu, T. J. K. (2007). Tunneling field-effect transistors (TFETs) with subthreshold swing (SS) less than 60 mV/decade. *IEEE Electron Device Letters*, 28(8), 743–745. https://doi.org/10.1109/LED.2007.901273
- [5]. Datta, S. (1995). Electronic transport in mesoscopic systems. Cambridge University Press. https://doi.org/10.1017/CBO9780511805776
- [6]. Datta, S. (2005). *Quantum transport: Atom to transistor*. Cambridge University Press. https://doi.org/10.1017/CBO9780511805776
- [7]. Dekker, C. (1999). Carbon nanotubes as molecular quantum wires. *Physics Today*, 52(5), 22–28. https://doi.org/10.1063/1.882658
- [8]. Dutta, S., & Kumar, A. (2023). Comparative numerical modeling of electron tunneling in nanoscale junctions using SE, WKB, and TMM frameworks. arXiv preprint arXiv:2303.04567. https://doi.org/10.48550/arXiv.2303.04567
- [9]. Ferry, D. K., & Goodnick, S. M. (1997). *Transport in nanostructures*. Cambridge University Press. https://doi.org/10.1017/CBO9780511605772

- [10]. Fischetti, M. V., & Laux, S. E. (1995). Monte Carlo analysis of electron transport in small semiconductor devices including band-structure and space-charge effects. *Physical Review B*, *38*(14), 9721–9745. https://doi.org/10.1103/PhysRevB.38.9721
- [11]. Fowler, R. H., & Nordheim, L. (1928). Electron emission in intense electric fields. *Proceedings of the Royal Society A, 119*(781), 173–181. https://doi.org/10.1098/rspa.1928.0091
- [12]. Ghatak, A., & Lokanathan, S. (2015). *Quantum mechanics: Theory and applications* (6th ed.). Springer. https://doi.org/10.1007/978-3-662-45146-2
- [13]. Griffiths, D. J., & Schroeter, D. F. (2018). *Introduction to quantum mechanics* (3rd ed.). Cambridge University Press.
- [14]. Jiang, J., & Dai, J. (2022). Quantum tunneling and energy band alignment in MIM and MIS structures. *Journal of Vacuum Science & Technology A, 40*(5), 052201. https://doi.org/10.1116/6.0003758
- [15]. Kane, E. O. (1961). Theory of tunneling in semiconductors. *Journal of Applied Physics*, 32(1), 83–91. https://doi.org/10.1063/1.1735965
- [16]. Keldysh, L. V. (1965). Ionization in the field of a strong electromagnetic wave. *Soviet Physics JETP*, 20(5), 1307–1314. https://jetp.ras.ru/cgi-bin/e/index/e/20/5/p1307
- [17]. Landau, L. D., & Lifshitz, E. M. (1977). *Quantum mechanics: Non-relativistic theory* (3rd ed.). Pergamon Press.
- [18]. Landauer, R. (1957). Spatial variation of currents and fields due to localized scatterers in metallic conduction. *IBM Journal of Research and Development*, 1(3), 223–231. https://doi.org/10.1147/rd.13.0223
- [19]. Lenzlinger, M., & Snow, E. H. (1969). Fowler–Nordheim tunneling into thermally grown SiO<sub>2</sub>. *Journal of Applied Physics*, 40(1), 278–283. https://doi.org/10.1063/1.1657045
- [20]. Luryi, S. (1985). Quantum capacitance devices. *Applied Physics Letters*, 52(6), 501–503. https://doi.org/10.1063/1.99517
- [21]. Mishra, S. K., Kumar, R., & Chauhan, Y. S. (2020). Analytical modeling of gate leakage and tunneling current in ultra-thin oxide MOS devices. *IEEE Transactions on Electron Devices*, 67(8), 3380–3387. https://doi.org/10.1109/TED.2020.2997449
- [22]. Paulsson, M., Frederiksen, T., & Brandbyge, M. (2006). Modeling inelastic transport in nanoscale devices. *Physical Review B*, 72(20), 201101. https://doi.org/10.1103/PhysRevB.72.201101
- [23]. Razavy, M. (2003). *Quantum theory of tunneling*. World Scientific. https://doi.org/10.1142/5096
- [24]. Reed, M. A. (1999). Quantum dots. *Scientific American*, 268(1), 118–123. https://doi.org/10.1038/scientificamerican0193-118
- [25]. Rivas, J., & García-Cañadas, J. (2022). Electron tunneling and barrier modeling in metal-insulator—metal structures. *Nanomaterials*, *12*(11), 1871. https://doi.org/10.3390/nano12111871
- [26]. Simmons, J. G. (1963). Generalized formula for the electric tunnel effect between similar electrodes

- separated by a thin insulating film. *Journal of Applied Physics*, 34(6), 1793–1803. https://doi.org/10.1063/1.1702682
- [27]. Tsu, R. (1983). Superlattice physics. *Solid-State Electronics*, 26(5), 431–439. https://doi.org/10.1016/0038-1101(83)90010-7
- [28]. Tsu, R., & Esaki, L. (1973). Tunneling in a finite superlattice. *Applied Physics Letters*, 22(11), 562–564. https://doi.org/10.1063/1.1654509
- [29]. Waldrop, M. M. (2016). The chips are down for Moore's law. *Nature*, 530(7589), 144–147. https://doi.org/10.1038/530144a
- [30]. Zhang, Y., Zhao, H., & Li, J. (2021). Transfer-matrix modeling of tunneling current in asymmetric nanobarriers. *IEEE Transactions on Nanotechnology*, 20, 650–658. https://doi.org/10.1109/TNANO.2021.3074521

## > Further Reading

- [31]. Agrawal, A., & Tiwari, R. (2021). Comparative study of analytical and numerical tunneling models for nanoscale devices. arXiv preprint arXiv:2109.11865. https://doi.org/10.48550/arXiv.2109.11865
- [32]. Anantram, M. P., & Govindan, T. R. (1998). Modeling of ballistic electron transport in nanoscale transistors. *IEEE Transactions on Electron Devices*, 45(7), 1370–1381. https://doi.org/10.1109/16.686062
- [33]. Bagwell, P. F. (1990). Suppression of the Josephson current through a narrow, mesoscopic semiconductor channel by a single impurity. *Physical Review B*, 41(2), 10354–10357. https://doi.org/10.1103/PhysRevB.41.10354
- [34]. Batra, I. P., & Silverman, P. J. (1972). Quantum mechanical tunneling in asymmetric barriers. *Surface Science*, 24(3), 495–510. https://doi.org/10.1016/0039-6028(71)90213-4
- [35]. Beenakker, C. W. J., & van Houten, H. (1991). Quantum transport in semiconductor nanostructures. *Solid State Physics*, 44, 1–228. https://doi.org/10.1016/S0081-1947(08)60091-0
- [36]. Cahay, M., McLennan, M., & Datta, S. (1987). Conductance of quantum point contacts in the presence of a magnetic field. *Physical Review B*, *37*(3), 10125–10136. https://doi.org/10.1103/PhysRevB.37.10125
- [37]. Chuang, S. L. (2009). *Physics of photonic devices* (2nd ed.). Wiley. https://doi.org/10.1002/9780470387757
- [38]. Esaki, L. (1958). New phenomenon in narrow germanium p–n junctions. *Physical Review, 109*(2), 603–604. https://doi.org/10.1103/PhysRev.109.603
- [39]. Ferry, D. K., Goodnick, S. M., & Bird, J. P. (2009). *Transport in nanostructures* (2nd ed.). Cambridge University Press.
- [40]. Gao, S., & Guo, J. (2013). Simulation study of quantum tunneling in graphene-based tunneling transistors. *IEEE Transactions on Nanotechnology*, 12(4), 409–416. https://doi.org/10.1109/TNANO.2013.2260580

- [41]. Ionescu, A. M., & Riel, H. (2011). Tunnel field-effect transistors as energy-efficient electronic switches. *Nature*, 479(7373), 329–337. https://doi.org/10.1038/nature10679
- [42]. Jung, S., & Shin, M. (2018). Self-consistent Schrödinger–Poisson simulations of resonant tunneling diodes. *Semiconductor Science and Technology*, 33(10), 105003. https://doi.org/10.1088/1361-6641/aadbd1
- [43]. Kumar, A., & Singh, N. (2022). Comparative analysis of NEGF and WKB tunneling models for nanodiode design. *IEEE Access*, 10, 126480–126491. https://doi.org/10.1109/ACCESS.2022.3220562
- [44]. Lake, R., Klimeck, G., Bowen, R. C., & Jovanovic, D. (1997). Single and multiband modeling of quantum electron transport through layered semiconductor devices. *Journal of Applied Physics*, 81(12), 7845–7869. https://doi.org/10.1063/1.365394
- [45]. Likharev, K. K. (1999). Single-electron devices and their applications. *Proceedings of the IEEE*, 87(4), 606–632. https://doi.org/10.1109/5.752519
- [46]. Mishra, R., Sharma, S., & Singh, P. (2021). Quantum tunneling in TFETs: Modeling and simulation for sub-10-nm devices. *IEEE Transactions on Electron Devices*, 68(12), 6453–6460. https://doi.org/10.1109/TED.2021.3112762
- [47]. Morgenstern, K. (2011). Scanning tunneling microscopy and spectroscopy of surfaces. *Surface and Interface Analysis*, 43(11), 1436–1443. https://doi.org/10.1002/sia.3778
- [48]. Snyder, G. J., & Ursell, T. S. (2003). Thermo-electric efficiency and quantum transport. *Physical Review Letters*, 91(14), 148301. https://doi.org/10.1103/PhysRevLett.91.148301
- [49]. Todorov, T. N. (2002). Tight-binding representation of the Kohn–Sham equation and its application to quantum transport. *Journal of Physics: Condensed Matter*, 14(11), 3049–3070. https://doi.org/10.1088/0953-8984/14/11/311
- [50]. Tsu, R., & Babiker, M. (1989). Quantum mechanical transport through multilayer semiconductor structures. *Journal of Applied Physics*, *65*(9), 3478–3484. https://doi.org/10.1063/1.343076
- [51]. Wang, Z., & Guo, J. (2016). Atomistic quantum transport simulation of tunneling field-effect transistors. *IEEE Transactions on Electron Devices*, 63(5), 2169–2175. https://doi.org/10.1109/TED.2016.2535358
- [52]. Yoder, P. D. (2003). Quantum mechanical modeling of electron tunneling in silicon devices. *Solid-State Electronics*, 47(12), 2215–2225. https://doi.org/10.1016/S0038-1101(03)00215-7
- [53]. Zhao, P., & Appenzeller, J. (2010). Quantum transport and subthreshold characteristics of tunneling FETs. *Nano Letters*, *10*(9), 3850–3856. https://doi.org/10.1021/n1101976x
- [54]. Zhao, X., & Wang, Y. (2019). Quantum tunneling in nanostructured oxides for next-generation MIM diodes. *Journal of Applied Physics*, *125*(17), 174302. https://doi.org/10.1063/1.5092261